[Research Paper] 대한금속 · 재료학회지 (*Korean J. Met. Mater.*), Vol. 61, No. 4 (2023) pp.277-283
DOI: 10.3365/KJMM.2023.61.4.277

Phase, Crystal Structure, and Thermoelectric Performance of Cubic Skinnerite $Cu_3Sb_{1-y}Fe_yS_3$ Synthesized by Mechanical Alloying

Sang Jun Park and Il-Ho Kim*

Department of Materials Science and Engineering, Korea National University of Transportation, Chungju 27469, Republic of Korea

Abstract: Skinnerite (Cu_3SbS_3) has recently attracted attention as a promising thermoelectric material because of its low thermal conductivity. In this study, we performed the solid-state synthesis of Fe-doped skinnerite $Cu_3Sb_{1-y}Fe_yS_3$ (y = 0.02–0.06) using mechanical alloying and hot pressing, and examined the samples' thermoelectric properties relative to Fe doping content. All samples contained only a cubic skinnerite phase, as evidenced by X-ray diffraction. As the Fe content increased, the lattice constant decreased from 1.03370 to 1.03310 nm, indicating successful substitution of Fe at the Sb sites. The carrier concentration increased with the Fe doping level, resulting in increased electrical conductivity. The specimens with y = 0.02–0.04 exhibited non-degenerate semiconductor behavior, where the electrical conductivity increased as the temperature increased. In contrast, a specimen with y = 0.06 changed conduction behavior to the degenerate state with minimal temperature dependence. As the Fe content increased, the Seebeck coefficient decreased, and $Cu_3Sb_{0.98}Fe_{0.02}S_3$ exhibited a maximum power factor of 1.16 $mWm^{-1}K^{-2}$ at 623 K. Thermal conductivity values for all specimens were lower than 1.20 $Wm^{-1}K^{-1}$ in the measured temperature range but were higher than undoped skinnerite. The highest thermoelectric performance was achieved by the $Cu_3Sb_{0.98}Fe_{0.02}S_3$ specimen, with a dimensionless figure of merit, ZT, of 0.9 obtained at 623 K.

(Received 5 December, 2022; Accepted 3 January, 2023)

Keywords: thermoelectric; skinnerite; mechanical alloying; hot pressing; doping

1. INTRODUCTION

Thermoelectric energy conversion technology offers a solution to the energy crisis, as it can directly convert heat into electricity and harvest thermal energy from low-grade heat sources [1-4]. The thermoelectric conversion efficiency depends on the performance of the thermoelectric material and the Carnot efficiency of the power generation system. The thermoelectric figure of merit is expressed as $Z = \alpha^2\sigma\kappa^{-1}$ [5], where the numerator term $\alpha^2\sigma$ is the power factor (α: Seebeck coefficient, σ: electrical conductivity, and κ: thermal conductivity). Because all three parameters (α, σ, and κ) are temperature-dependent, the dimensionless index (ZT) is used to evaluate the thermoelectric properties by multiplying the absolute temperature (T). Therefore, to improve the performance of thermoelectric materials, it is necessary to increase their power factor at the application temperature and/or decrease their thermal conductivity.

Recently, Cu-Sb-S compounds have been attracting interest as eco-friendly and cost-effective energy materials. Four types of compounds are candidates for p-type thermoelectric materials: Cu_3SbS_4 (famatinite), $Cu_{12}Sb_4S_{13}$ (tetrahedrite), Cu_3SbS_3 (skinnerite), and $CuSbS_2$ (chalcostibite). Except for Cu_3SbS_4, these compounds are known to have low lattice thermal conductivity because the Cu atoms vibrate because of the unshared electron pairs (lone-pair electrons) of Sb. Among the Cu-Sb-S compounds, Cu_3SbS_3 has the largest S-Sb-S bonding angle, and thus the lowest lattice thermal conductivity [6]. In addition, it has a high absorption coefficient and a suitable bandgap energy (1.40–1.84 eV) for photovoltaic applications [7-10]. However, there have been few studies on the thermoelectric performance of Cu_3SbS_3.

Skinnerite is known to have three crystal structures [11,12]: orthorhombic (space group $P2_12_12_1$, <263 K), monoclinic (space group $P2_1/c$, 263–395 K), and orthorhombic (space group Pnma, >395 K). These structural phase transitions arise

- 박상준: 학사과정, 김일호: 교수
*Corresponding Author: Il-Ho Kim
[Tel: +82-10-5338-1582, E-mail: ihkim@ut.ac.kr]

because of the disorderly motion of Cu atoms as the temperature increases. Skinnerite synthesized by the conventional melting method has a monoclinic structure at room temperature, but when the temperature is elevated to 395 K or higher, the phase is transformed from monoclinic to orthorhombic; thus, its application as a thermoelectric material may be limited [13]. In addition to these three known structures, skinnerite may form a cubic structure, which is predicted to be similar to tetrahedrite ($Cu_{12}Sb_4S_{13}$ or $Cu_3SbS_{3.25}$) [14]. Cubic skinnerite maintains lone-pair electrons in a tetrahedron at the Sb site but has no S atom at the center of the unit cell and is missing a S atom at the CuS_3 triangular vertex. This structure is unstable, which can have a significant effect on the vibrational mode of the triangulated Cu atoms and Sb atoms with lone-pair electrons [13]. Du et al. [14] stabilized the cubic skinnerite phase by partially replacing Sb with Fe. The effect of Fe doping on the crystal structure has also been reported for Cu-Fe-Sb-S quaternary systems [15,16].

In our previous studies [17,18], we synthesized a cubic skinnerite Cu_3SbS_3 phase stable at 323−623 K using mechanical alloying (MA) followed by hot pressing (HP), and a good thermoelectric performance (ZT = 0.51 at 623 K) was obtained. In this study, we prepared Fe-doped $Cu_3Sb_{1-y}Fe_yS_3$ using the MA-HP process and evaluated the effect of the Fe doping level on the thermoelectric properties.

2. EXPERIMENTAL PROCEDURE

To synthesize $Cu_3Sb_{1-y}Fe_yS_3$ (y = 0.02, 0.04, and 0.06), elemental powders of Cu (purity 99.9%, <45 μm), Sb (purity 99.999%, <75 μm), Fe (purity 99.9%, <53 μm), and S (purity 99.99%, <75 μm) were weighed to stoichiometric compositions, and the mixed raw powders and stainless-steel balls were loaded into a hardened steel jar. MA was conducted at 350 rpm for 18 h in an Ar atmosphere using a planetary ball mill (Fritsch, Pulverisette5). The synthesized powder was loaded into a graphite mold and HP was performed under a pressure of 70 MPa at 623 K for 2 h. The optimal MA-HP process conditions were determined in our previous studies [17,18].

The phases of the MA powder and HP sintered bodies were analyzed using X-ray diffraction (XRD; Bruker, D8-Advance) with Cu Kα radiation. The Rietveld analysis program (TOPAS) was used to calculate the lattice constants. The microstructure of the sintered specimens was observed using scanning electron microscopy (SEM; FEI, Quanta400) in the backscattered electron mode (BSE). Elemental line scanning and mapping analyses were performed according to the energy level of each element using energy-dispersive X-ray spectroscopy (EDS; Bruker, XFlash4010). Carrier concentration and mobility were evaluated by measuring the Hall coefficient using the van der Pauw method (Keithley 7065). The Seebeck coefficient and electrical conductivity were measured using ZEM-3 equipment (Advance Riko) in a He atmosphere, and the thermoelectric power factor was examined. The thermal diffusivity, specific heat, and density were measured using a TC-9000H system (Advance Riko) in a vacuum atmosphere, and the thermal conductivity was estimated. The temperature dependence of the thermoelectric characteristics was examined over the temperature range of 323–623 K using the measured Seebeck coefficient, electrical conductivity, and thermal conductivity. Finally, the dimensionless figure of merit was evaluated.

3. RESULTS AND DISCUSSION

Figure 1(a) shows the XRD patterns of the $Cu_3Sb_{1-y}Fe_yS_3$ powders synthesized by MA. Cubic skinnerite (space group $I\bar{4}3$ m: PDF#01-075-1574) was obtained after MA at 350 rpm for 18 h. The MA powder was confirmed to have a single cubic skinnerite phase. Figure 1(b) shows the XRD patterns of the $Cu_3Sb_{1-y}Fe_yS_3$ specimens sintered by HP. The cubic skinnerite phase remained even after HP at 623 K under 70 MPa, without phase decomposition or phase transitions. The lattice constants calculated by Rietveld analysis are summarized in Table 1, confirming the substitution of Fe at the Sb sites. The lattice constant of undoped cubic Cu_3SbS_3, reported by Lee [17,18] was 1.03740 nm. However, in this study, the lattice constant was significantly reduced by Fe doping. This is because the ionic radius of Fe is smaller than that of Sb. Shannon [19] reported ionic radii of 90, 76, and 63 pm for Sb^{3+}, Fe^{2+}, and Fe^{3+}, respectively. Zhang et al. [13] reported that Fe (117 pm) had a smaller covalent radius than Sb (140 pm). In this study, as the Fe content increased, the lattice constant decreased from 1.03370 to 1.03310 nm, indicating the successful substitution

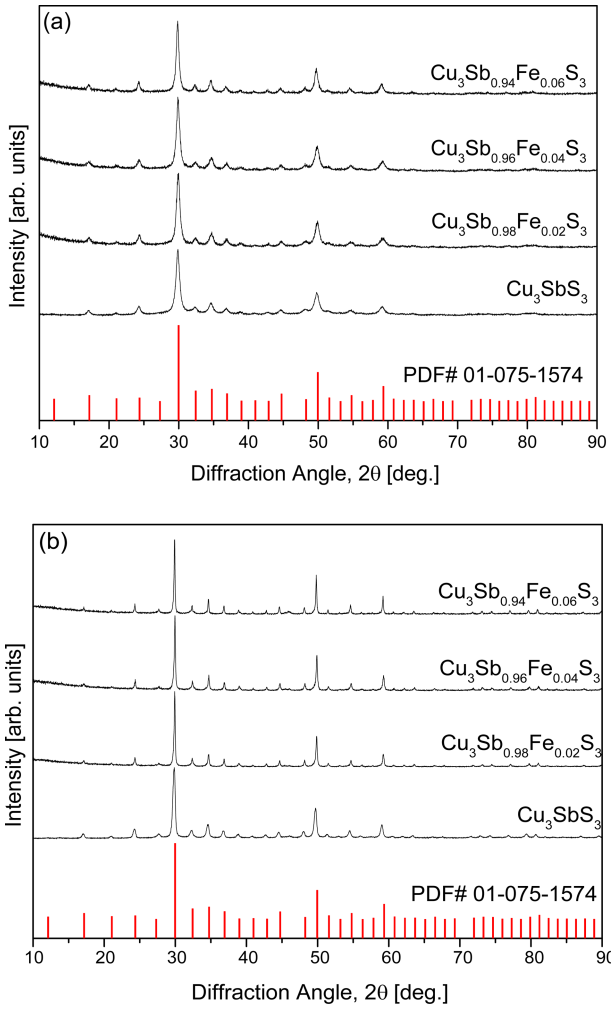

Fig. 1. XRD patterns of (a) synthetic powders and (b) sintered specimens of $Cu_3Sb_{1-y}Fe_yS_3$.

Table 1. Relative densities and lattice constants of $Cu_3Sb_{1-y}Fe_yS_3$.

Specimen	Relative density [%]	Lattice constant [nm]
Cu_3SbS_3	99.7	1.03740
$Cu_3Sb_{0.98}Fe_{0.02}S_3$	98.8	1.03370
$Cu_3Sb_{0.96}Fe_{0.04}S_3$	98.3	1.03366
$Cu_3Sb_{0.94}Fe_{0.06}S_3$	98.6	1.03310

of Fe at the Sb sites.

For comparison, the data [17,18] for undoped Cu_3SbS_3 are shown in Table 1 and Figs. 1–9. Du et al. [14] detected a secondary phase of $Cu_{2-x}S$ and could not obtain single-phase cubic Cu_3SbS_3 by heat treatment without the addition of a proper dopant, although cubic Cu_3SbS_3 was synthesized by MA and spark plasma sintering (SPS). Pfitzner [12] synthesized stable orthorhombic Cu_3SbS_3 (space group Pnma) at temperatures higher than 394 K by vacuum melting of Cu_2S and Sb_2S_3, but cubic Cu_3SbS_3 could not be synthesized. Daniel et al. [20] reported that a Cu_3SbS_3 thin film produced by thermal evaporation had a monoclinic structure (space group $P2_1/c$). Even after annealing at temperatures up to 573 K, the crystallinity improved but there was no change in the crystal structure. Wang et al. [21] reported that Cu_3SbS_3 nanowires synthesized by a solvothermal route exhibited an orthorhombic structure. Atri et al. [22] obtained cubic skinnerite (space group $I\bar{4}3$ m) via co-thermal deposition and wet-chemical synthesis for non-stoichiometric (Cu-poor or Cu-rich) compositions. However, they found the crystal structure changed to orthorhombic in the case of $Cu_3Bi_{0.5}Sb_{0.5}S_3$, when Bi was substituted at the Sb site, due to the expansion of the unit cell since Bi^{3+} has a larger ionic radius than Sb^{3+}.

Figure 2 presents SEM photographs and EDS analysis results of the sintered specimens of $Cu_3Sb_{1-y}Fe_yS_3$. High sintered densities (relative densities) of 98.3%–98.8% were obtained (Table 1) compared to the theoretical density (5.1 gcm^{-3}) of Cu_3SbS_3 [12]. Figure 2(a) shows the polished surfaces of $Cu_3Sb_{0.98}Fe_{0.02}S_3$ with the elemental line scans. Figures 2(b)–2(d) show the fractured surfaces of sintered $Cu_3Sb_{1-y}Fe_yS_3$ (y = 0.02–0.06). No specific changes in the microstructure are observed with respect to the Fe content. Figures 2(e)–2(h) present the elemental distributions in the specimen with y = 0.02 and show that all elements are homogeneously distributed.

Figure 3 shows the charge transport properties (carrier concentration and mobility) of $Cu_3Sb_{1-y}Fe_yS$. Hall coefficient measurements confirmed that all specimens were p-type semiconductors with positive Hall coefficients; this data is not presented. Cu vacancies with low formation energies are easily formed in Cu chalcogenide compounds and contribute to the p-type conduction behavior [23]. Undoped cubic Cu_3SbS_3 has a carrier (hole) concentration of (3.3–3.9) × 10^{18} cm^{-3} and mobility of 146–153 $cm^2V^{-1}s^{-1}$ [17,18]. However, in this study, Fe doping increased the carrier concentration to (1.2–1.7) × 10^{19} cm^{-3}, and the mobility was in the range of 248–392 $cm^2V^{-1}s^{-1}$ on average. In skinnerite, Sb exists as Sb^{3+}, and the dopant Fe may exist as Fe^{2+} or Fe^{3+}. Considering the increase in the hole concentration due to Fe doping, we conclude that Sb^{3+} is substituted with Fe^{2+}. Zhang

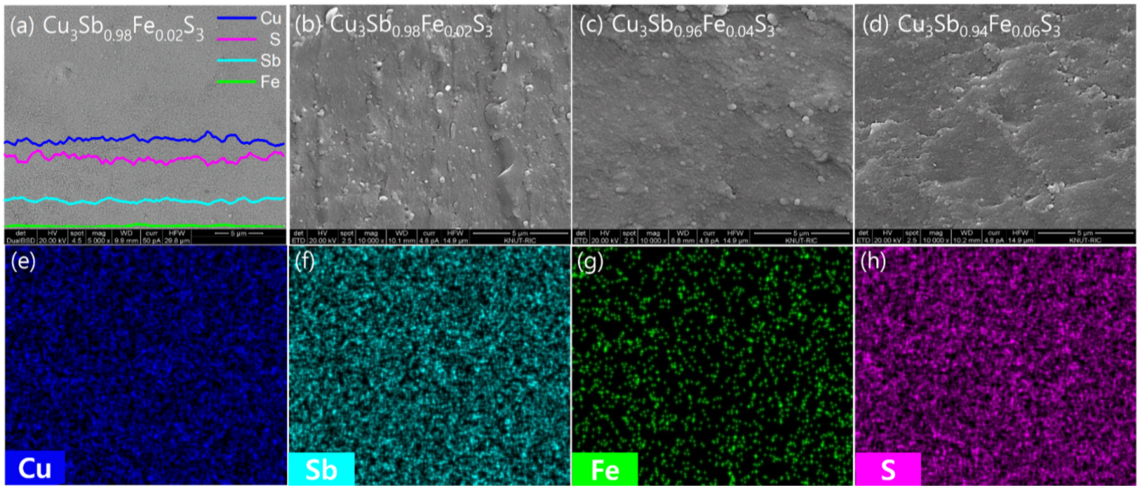

Fig. 2. SEM images of the (a) polished surface with EDS elemental line scans, (b-d) fractured surfaces of $Cu_3Sb_{1-y}Fe_yS_3$, and (e-h) EDS elemental maps of $Cu_3Sb_{0.98}Fe_{0.02}S_3$.

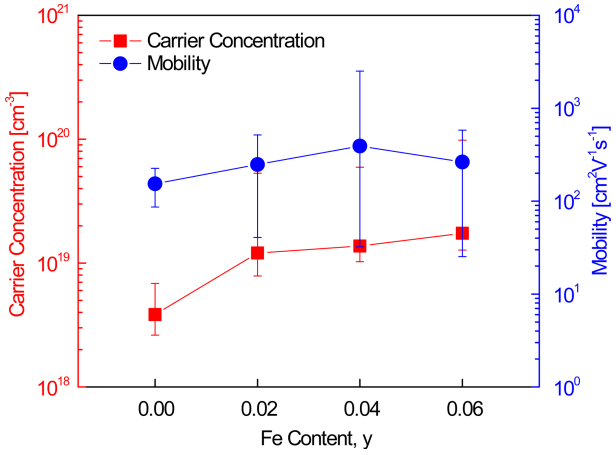

Fig. 3. Charge transport properties of $Cu_3Sb_{1-y}Fe_yS_3$.

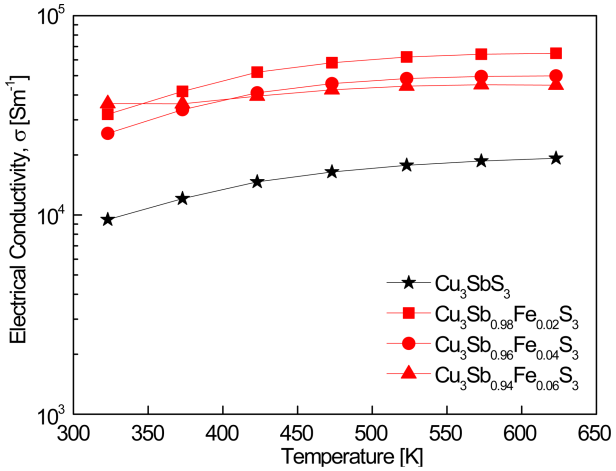

Fig. 4. Temperature dependence of the electrical conductivity for $Cu_3Sb_{1-y}Fe_yS_3$.

et al. [13] obtained a hole concentration of 6.5×10^{19} cm^{-3} and mobility of 2.4 cm^{2}V^{-1}s^{-1} for cubic Cu_3SbS_3, and a hole concentration of 1.9×10^{20} cm^{-3} and mobility of 5.8 cm^{2}V^{-1}s^{-1} for cubic $Cu_3Sb_{0.9}Fe_{0.1}S_3$. Du et al. [14] reported a hole concentration of 9.1×10^{19} cm^{-3} and mobility of 3.7 cm^{2}V^{-1}s^{-1} for orthorhombic Cu_3SbS_3 (in reality, orthorhombic skinnerite + cubic tetrahedrite), and a hole concentration of 3.2×10^{20} cm^{-3} and mobility of 16 cm^{2}V^{-1}s^{-1} for cubic $Cu_3Sb_{0.9}Fe_{0.1}S_3$, similar to values obtained for cubic tetrahedrite.

Figure 4 shows the electrical conductivity of $Cu_3Sb_{1-y}Fe_yS_3$. Cubic Cu_3SbS_3 exhibits an electrical conductivity of $(0.95–1.92) \times 10^4$ Sm^{-1} at 323–623 K, but Fe doping increased this to $(2.55–3.62) \times 10^4$ Sm^{-1} at 323 K and $(4.48–6.47) \times 10^4$ Sm^{-1} at 623 K, indicating non-degenerate semiconductor behavior. However, as the Fe content increases, the temperature dependence of the electrical conductivity decreases. Chen et al. [6] obtained a very low electrical conductivity of approximately 10 Sm^{-1} at 300 K for orthorhombic Cu_3SbS_3, owing to the low carrier concentration. Zhang et al. [13] reported an electrical conductivity of $(0.25–2.00) \times 10^4$ Sm^{-1} for cubic Cu_3SbS_3 and $(1.75–3.57) \times 10^4$ Sm^{-1} for cubic $Cu_3Sb_{0.9}Fe_{0.1}S_3$ at 323–623 K. Du et al. [14] achieved $(0.54–1.63) \times 10^3$ Sm^{-1} for orthorhombic Cu_3SbS_3 and $(0.81–2.00) \times 10^4$ Sm^{-1} for cubic $Cu_3Sb_{0.9}Fe_{0.1}S_3$ at 300–625 K.

Figure 5 shows the Seebeck coefficients of $Cu_3Sb_{1-y}Fe_yS_3$. Lee [17,18] obtained a Seebeck coefficient of 140–178 μVK^{-1}

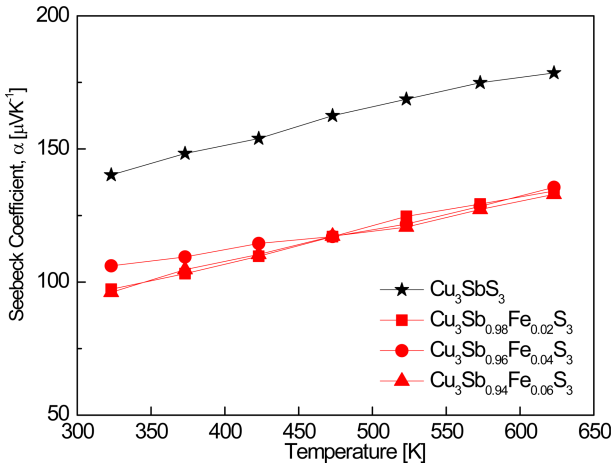

Fig. 5. Temperature dependence of the Seebeck coefficient for $Cu_3Sb_{1-y}Fe_yS_3$.

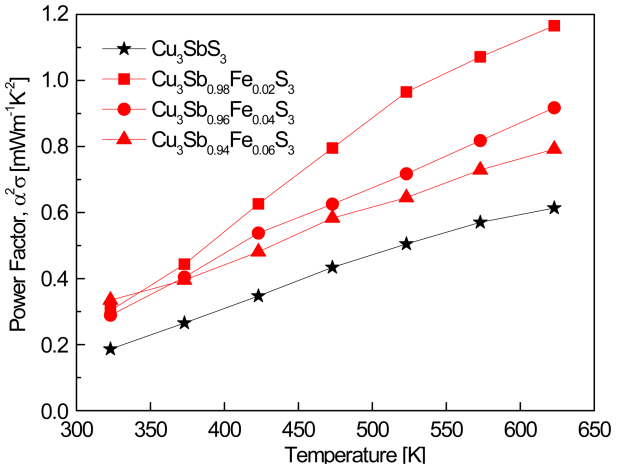

Fig. 6. Temperature dependence of the power factor for $Cu_3Sb_{1-y}Fe_yS_3$.

at 323–623 K for cubic Cu_3SbS_3. However, in this study, Fe doping lowered the Seebeck coefficient to 97–106 μVK^{-1} at 323–623 K for $Cu_3Sb_{0.94}Fe_{0.06}S_3$. This was attributed to the increase in the carrier concentration caused by Fe doping. When the temperature increased in the measurement temperature range, the Seebeck coefficient gradually increased; an intrinsic transition did not occur. The positive Seebeck coefficient confirms that the Fe-doped skinnerite acts as a p-type semiconductor. Zhang et al. [13] reported Seebeck coefficients of 177–180 μVK^{-1} for cubic Cu_3SbS_3 and 114–162 μVK^{-1} for cubic $Cu_3Sb_{0.9}Fe_{0.1}S_3$ at 300–623 K. Du et al. [14] obtained values of 165–220 μVK^{-1} for orthorhombic Cu_3SbS_3 and 165–180 μVK^{-1} for cubic $Cu_3Sb_{0.9}Fe_{0.1}S_3$ at 300–625 K, which were higher than the 115–145 μVK^{-1} reported for tetrahedrite at the same temperatures.

Figure 6 shows the temperature dependence of the thermoelectric power factor of $Cu_3Sb_{1-y}Fe_yS_3$. Cubic Cu_3SbS_3 exhibited a power factor of 0.17–0.61 $mWm^{-1}K^{-2}$ at 323–623 K; however, this was greatly improved by doping with Fe to 0.28–0.33 $mWm^{-1}K^{-2}$ at 323 K and 0.79–1.17 $mWm^{-1}K^{-2}$ at 623 K. This results from a significant increase in electrical conductivity, although there was a decrease in the Seebeck coefficient because of Fe doping. $Cu_3Sb_{0.98}Fe_{0.02}S_3$ exhibited a maximum power factor of 1.17 $mWm^{-1}K^{-2}$ at 623 K. Du et al. [14] reported a low power factor of 0.077 $mWm^{-1}K^{-2}$ at 625 K for orthorhombic Cu_3SbS_3 but obtained a 10-fold increased value of 0.627 $mWm^{-1}K^{-2}$ at 625 K for cubic

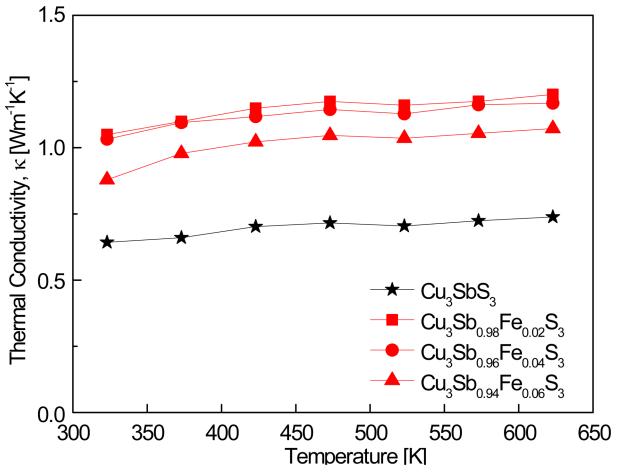

Fig. 7. Temperature dependence of the thermal conductivity for $Cu_3Sb_{1-y}Fe_yS_3$.

$Cu_3Sb_{0.9}Fe_{0.1}S_3$. As a result, Fe doping at skinnerite was suggested to improve the power factor; however, this value is lower than 1.04 $mWm^{-1}K^{-2}$ at 625 K for the tetrahedrite produced by the same MA-HP method.

Figure 7 shows the thermal conductivity of $Cu_3Sb_{1-y}Fe_yS_3$. Cubic Cu_3SbS_3 exhibits a thermal conductivity of 0.64–0.74 $Wm^{-1}K^{-1}$ at 323–623 K; however, cubic $Cu_3Sb_{1-y}Fe_yS_3$ (y = 0.02–0.06) reached a higher thermal conductivity of 0.88–1.05 $Wm^{-1}K^{-1}$ at 323 K and 1.07–1.20 $Wm^{-1}K^{-1}$ at 623 K. Zhang et al. [13] obtained a thermal conductivity of 0.45–0.70 $Wm^{-1}K^{-1}$ for cubic Cu_3SbS_3 and 0.55–0.95 $Wm^{-1}K^{-1}$ for cubic $Cu_3Sb_{0.9}Fe_{0.1}S_3$ at 300–623 K. Du et al. [14] reported 0.30–0.25 $Wm^{-1}K^{-1}$ for orthorhombic Cu_3SbS_3; Fe doping

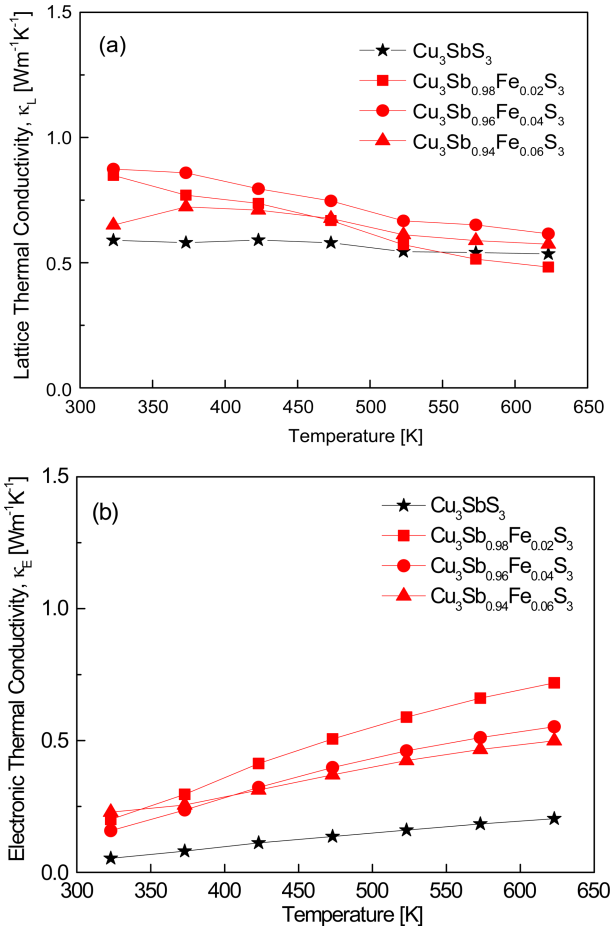

Fig. 8. Separation of the (a) lattice thermal conductivity and (b) electronic thermal conductivity.

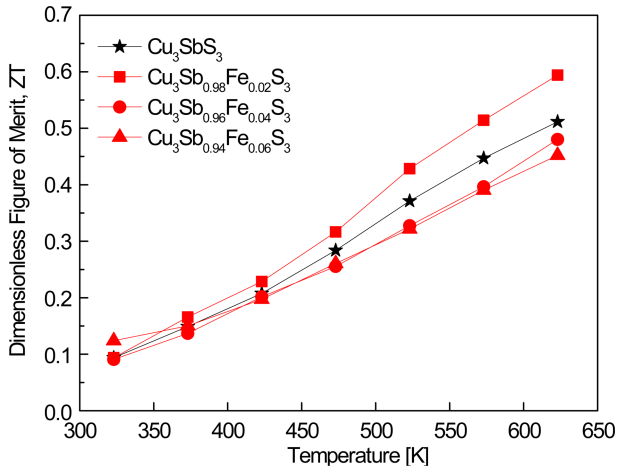

Fig. 9. Dimensionless figure of merit for $Cu_3Sb_{1-y}Fe_yS_3$.

increased this to 0.45–0.55 Wm^{-1}K^{-1} for cubic $Cu_3Sb_{0.9}Fe_{0.1}S_3$ at 300–625 K. However, these values are lower than the 0.85–0.95 Wm^{-1}K^{-1} obtained for tetrahedrite at the same temperatures.

Figure 8 shows the lattice and electronic thermal conductivities of $Cu_3Sb_{1-y}Fe_yS_3$. Assuming no bipolar conduction, thermal conductivity can be expressed as the sum of the lattice thermal conductivity (κ_L) by phonon transport and the electronic thermal conductivity (κ_E) of the charge carriers. Here, the electronic thermal conductivity was calculated using the Wiedemann–Franz relation ($\kappa_E = L\sigma T$). The temperature-dependent Lorenz number (L) was calculated using the formula $L = 1.5 + exp(-|\alpha|/116)$ [24]. Lee [17,18] reported κ_L = 0.53–0.59 Wm^{-1}K^{-1} and κ_E = 0.05–0.20 Wm^{-1}K^{-1} for cubic Cu_3SbS_3 at 323–623 K. In this study, cubic $Cu_3Sb_{1-y}Fe_yS_3$ (y = 0.02–0.06) exhibited κ_L = 0.65–0.87 Wm^{-1}K^{-1} and κ_E = 0.16–0.23 Wm^{-1}K^{-1} at 323 K, and κ_L = 0.48–0.62 Wm^{-1}K^{-1} and κ_E = 0.50–0.72 Wm^{-1}K^{-1} at 623 K. Zhang et al. [13] reported κ_L = 0.45–0.40 Wm^{-1}K^{-1} for cubic Cu_3SbS_3 and κ_L = 0.61–0.36 Wm^{-1}K^{-1} for cubic $Cu_3Sb_{0.9}Fe_{0.1}S_3$ at 300–623 K. Du et al. [14] obtained κ_L = 0.30–0.20 Wm^{-1}K^{-1} for orthorhombic Cu_3SbS_3 and κ_L = 0.40–0.25 Wm^{-1}K^{-1} for cubic $Cu_3Sb_{0.9}Fe_{0.1}S_3$ at 300–625 K, which is lower than κ_L = 0.75–0.40 Wm^{-1}K^{-1} for tetrahedrite at 300–625 K.

Figure 9 shows the temperature dependence of the ZT values for $Cu_3Sb_{1-y}Fe_yS_3$. The ZT value increased with temperature because of the temperature dependence of the power factor and thermal conductivity. The ZT values of the Fe-doped cubic skinnerites $Cu_3Sb_{1-y}Fe_yS_3$ (y = 0.02–0.06) ranged from 0.09–0.12 at 323 K to 0.59–0.45 at 623 K. In our previous studies [17,18], cubic Cu_3SbS_3 prepared by the MA-HP process exhibited a maximum ZT of 0.51 at 623 K. However, in this study, Fe doping stabilized the cubic skinnerite phase and improved the thermoelectric performance; as a result, ZT = 0.59 was achieved at 623 K for $Cu_3Sb_{0.9}Fe_{0.02}S_3$. Zhang et al. [13] reported a ZT = 0.57 for cubic Cu_3SbS_3 and ZT = 0.62 for cubic $Cu_3Sb_{0.9}Fe_{0.1}S_3$ produced by the MA-HP-annealing-quenching process at 623 K. Du et al. [14] obtained a low value of ZT = 0.1 at 623 K for orthorhombic Cu_3SbS_3 produced by the MA-HP method, but the thermoelectric performance was greatly improved by Fe doping, resulting in ZT = 0.25–0.70 at 623 K for cubic $Cu_3Sb_{1-y}Fe_yS_3$ (y = 0.02–0.1).

4. CONCLUSIONS

Cubic skinnerites $Cu_3Sb_{1-y}Fe_yS_3$ ($0.02 \leq y \leq 0.06$) were successfully synthesized using MA and HP. From the results of the XRD phase identification and SEM–EDS analysis, Fe doping was effective in creating a single skinnerite phase with a cubic structure. However, no skinnerite phases with monoclinic or orthorhombic structures were produced. The HP was performed at 623 K to obtain homogeneous and densely sintered bodies. The cubic skinnerite phase remained after HP without changes in the crystal structure, phase transition, or phase decomposition. The Fe-doped skinnerites behaved like p-type semiconductors; $Cu_3Sb_{0.98}Fe_{0.02}S_3$ and $Cu_3Sb_{0.96}Fe_{0.04}S_3$ exhibited non-degenerate semiconductor behavior, whereas $Cu_3Sb_{0.94}Fe_{0.06}S_3$ exhibited degenerate semiconductor behavior with minimal temperature dependence on electrical conductivity. Fe doping at the Sb sites increased the carrier concentration, resulting in an increase in electrical conductivity and a decrease in the Seebeck coefficient. An increase in the electronic thermal conductivity by Fe doping resulted in an increase in thermal conductivity, and a thermal conductivity of 0.85–1.20 $Wm^{-1}K^{-1}$ was obtained at 323–623 K. $Cu_3Sb_{0.98}Fe_{0.02}S_3$ exhibited a maximum power factor of 1.16 $mWm^{-1}K^{-2}$ and the highest ZT of 0.59 at 623 K. In summary, a single Fe-doped cubic skinnerite phase was prepared by the MA-HP process without subsequent annealing, and the partial doping of Fe at the Sb sites was effective in stabilizing the skinnerite phase and improving thermoelectric performance. We conclude that skinnerite has potential as a thermoelectric material for mid-temperature applications.

Acknowledgments

This study was supported by the Basic Science Research Capacity Enhancement Project (National Research Facilities and Equipment Center) through the Korea Basic Science Institute funded by the Ministry of Education (Grant No. 2019R1A6C1010047).

REFERENCES

1. X. Zhou, Y. Yan, X. Lu, H. Zhu, X. Han, G. Chen, and Z. Ren, *Mater. Today* **21**, 974 (2018).
2. O. H. Ando Junior, A. L. O. Maran, and N. C. Henao, *Renew. Sustain. Energy Rev.* **91**, 376 (2018).
3. A. V. Powell, *J. Appl. Phys.* **126**, 100901 (2019).
4. C. Baday, M. Yurddaskal, M. Ozgul, M. Zor, and E. Celik, *J. Mater. Sci.* **28**, 17468 (2017).
5. X. Lu, D. T. Morelli, Y. Xia, F. Zhou, V. Ozolins, H. Chi, X. Zhou, and C. Uher, *Adv. Energy Mater.* **3**, 342 (2012).
6. K. Chen, *Synthesis and Thermoelectric Properties of Cu-Sb-S Compounds*, Ph.D. Thesis (United Kingdom: Queen Mary University of London, 2016).
7. P. Maiello, G. Zoppi, W. R. Miles, N. Pearsall, and I. Forbes, *Sol. Energy Mater. Sol. Cells* **113**, 186 (2013).
8. K. Ramasamy, H. Sims, W. H. Butler, and A. Gupta, *Chem. Mater.* **26**, 2891 (2014).
9. K. Nefzi, A. Rabhi, and M. Kanzari, *J. Mater. Sci.: Mater. Electron.* **27**, 1888 (2016).
10. A. Hussain, R. Ahmed, N. Ali, A. Shaari, J. T. Luo, and Y. Q. Fu, *Surf. Coat. Technol.* **319**, 294 (2017).
11. H. J. Whitfield, *Sol. Sta. Commun.* **33**, 747 (1980).
12. A. Pfitzner, *Z. Kristallogr.* **213**, 228 (1998).
13. J. Zhang, L. Wang, M. Liu, J. Wang, K. Sun, Y. Yang, B. Hu, J. Xu, T. Su, and B. Du, *J. Mater. Sci.: Mater. Electron.* **32**, 10789 (2021).
14. B. Du, R. Zhang, M. Liu, K. Chen, H. Zhang, and M. J. Reece, *J. Mater. Chem. C* **7**, 394 (2019).
15. K. Tatsuka and N. Morimoto, *Econ. Geol.* **72**, 258 (1977).
16. V. Raghavan, *J. Phase Equilib. Diffus.* **25**, 459 (2004).
17. G. E. Lee, *Thermoelectric Properties of $Cu_3Sb(S/Se)_4$ and $Cu_3Sb(S/Se)_3$ Prepared by Solid-state Synthesis*, Ph.D. Thesis (Republic of Korea: Korea National University of Transportation, 2021).
18. G. E. Lee and I. H. Kim, *Korean J. Met. Mater.* **60**, 455 (2022).
19. R. D. Shannon, *Acta Crystallogr. A* **32**, 751 (1976).
20. T. Daniel, K. Mohanraj, and G. Sivakumar, *J. Mater. Sci.: Mater. Electron.* **29**, 9251 (2018).
21. M. X. Wang, G. H. Yue, X. Y. Fan, and P. X. Yan, *J. Cryst. Grow.* **310**, 3062 (2008).
22. S. Atri, M. Gusain, P. Kumar, S. Uma, and R. Nagarajan, *J. Chem. Sci.* **132**, 132 (2010).
23. C. Yang, F. Huang, L. Wu, and K. Xu, *J. Phys. D: Appl. Phys.* **44**, 295404 (2011).
24. H. S. Kim, Z. M. Gibbs, Y. Tang, H. Wang, and G. J. Snyder, *APL Mater.* **3**, 041506 (2015).